BIOCHEMISTRY
including biophysical chemistry & molecular biology

Article

pubs.acs.org/biochemistry

How the Ankyrin and SOCS Box Protein, ASB9, Binds to Creatine Kinase

Deepa Balasubramaniam, Jamie Schiffer, Jonathan Parnell, Stephan P. Mir, Rommie E. Amaro, and Elizabeth A. Komives*

Department of Chemistry and Biochemistry, University of California, San Diego, 9500 Gilman Drive, La Jolla, California 92093-0378, United States

Supporting Information

ABSTRACT: The ankyrin repeat and SOCS box (ASB) family is composed of 18 proteins and belongs to the suppressor of cytokine signaling (SOCS) box protein superfamily. The ASB proteins function as the substrate-recognition subunits of ECS-type (ElonginBC-Cullin-SOCS-box) Cullin RING E3 ubiquitin ligase (CRL) complexes that specifically transfer ubiquitin to cellular proteins targeting them for degradation by the proteasome. ASB9 binds to creatine kinase (CK) and targets it for degradation; however, the way in which ASB9 interacts with CK is not yet known. We present a complete characterization of the binding of ASB9 to CK. One ASB9 molecule binds to a dimer of CK. The binding affinity of ASB9(1−252) was extremely tight, and no dissociation could be observed. Deletion of the 34 N-terminal amino acids forming ASB9(35−252) resulted in weakening of the binding, so that a binding affinity of 2.6 nM could be measured. Amide hydrogen−deuterium exchange (HDXMS) experiments showed that both ASB9(1−252) and ASB9(35−252) protected the same region of CK, residues 182−203, which forms one side of the active site. The HDXMS experiments indicated that the N-terminal disordered region and first ankyrin repeat of ASB9 are protected from exchange in the complex. Molecular docking yielded a structural model consistent with all of the data that suggested the N-terminal residues of ASB9(1−252) may lie in one CK active site. This model was corroborated by enzymatic activity assays and mutational analysis.

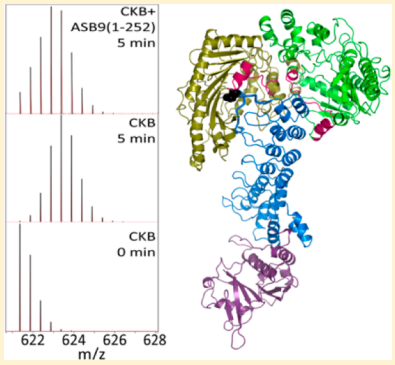

Proteasome-dependent protein degradation occurs when ubiquitin is transferred to the ε-amine of lysine residues within the doomed protein.[1,2] The transfer of ubiquitin requires a three-enzyme system comprised of an E1 ubiquitin-activating enzyme, an E2 ubiquitin-conjugating enzyme, and an E3 ubiquitin ligase. It is the E3 ligase that binds the doomed protein, brings it together with the E2 enzyme, and catalyzes the transfer of ubiquitin. More than 600 human E3 ligases have been identified. The most well-characterized is the SCF family, for which structures have been available for more than 10 years.[3] The Cullin RING E3 ligases (CRL) make up the largest family of E3 ligases in eukaryotes and have separate substrate-binding and catalytic subunits.[4,5] The substrate-recognition protein binds to the N-terminal domain of the Cullin subunit (Cul1−5 or Cul7), and a RING protein (Rbx1 or Rbx2), which in turn recruits the E2 ubiquitin conjugate, binds to the C-terminal domain. Neddylation of the Cullin C-terminal domain is thought to alter the conformation, so that the substrate and ubiquitin are brought into the proximity of each other.[6]

The ankyrin repeat and SOCS box (ASB) family is composed of 18 proteins and belongs to the suppressor of cytokine signaling (SOCS) box protein superfamily. The ASB proteins interact with Cul5-Rbx2 to form a functional E3 ubiquitin ligase.[7] ASB family members function as the substrate-recognition subunits of ECS-type (ElonginBC-Cullin-SOCS-box) Cullin RING E3 ubiquitin ligase (CRL) complexes that specifically transfer ubiquitin to cellular proteins targeting them for degradation by the proteasome. The quaternary multi-subunit complex formed by ASB9, Elongin B, Elongin C (EloBC), and Cullin 5 was recently characterized,[8] and the structure of ASB9 bound to Elongins B and C has also been reported.[9] However, the interactions of the ASB subunits with their substrates and the assembly of the ASB subunits within ECS-type ubiquitin ligases remain poorly understood.

The Elongin BC, Cullin 5, and Rbx2 proteins are the same for each ASB-containing CRL, so it is thought that the ASB protein is responsible for binding the target protein and that each ASB binds to a different target protein. The ASBs are composed of an N-terminal ankyrin repeat domain (ARD) with different numbers of ankyrin repeats, and a C-terminal SOCS box domain.[7] ASB proteins bind and recognize their specific substrate through the ARD. The CRL containing ASB9 binds to creatine kinase (CK) and targets it for degradation;[10,11] however, the way in which ASB9 interacts with CK is not yet known. The structure of ASB9 (residues 37−294) bound to Elongin BC[9] and the structure of ASB9 (residues 19−252)[12,13] both show similar architectures of the well-folded ARD of ASB9. Interestingly, a sequence C-terminal to the ARD appears

Received: November 16, 2014
Revised: February 2, 2015
Published: February 5, 2015

DOI: 10.1021/bi501420n
Biochemistry 2015, 54, 1673−1680

to form part of an additional ankyrin repeat. A structural model for the ASB9−CK interaction was proposed on the basis of the way in which other ankyrin repeat proteins bind their targets; however, the experimental evidence for this model would also have been consistent with a variety of interaction modes.[13]

ASB9 is predominantly expressed in the kidney and testes, and it has been shown to bind to and ubiquitinate brain-type cytosolic creatine kinase (CKB)[10] and ubiquitous mitochondrial creatine kinase (uMtCK).[11] Recent evidence suggests that ASB9 could be a biomarker for human breast cancer,[14] and it has also been linked to colorectal cancer.[15] The reduction of the level of uMtCK expression by siRNA led to an increased rate of cell death, and reduced rates of proliferation, migration, and invasion in HCC cell lines. Transient overexpression of ASB9 reduced uMtCK protein levels in HCC cells, suggesting that the increased uMtCK levels that correlate with poor prognosis may be due to a reduced level of ASB9 expression.[16]

We present the complete characterization of the binding of ASB9 to CK, including measurement of the binding affinity and stoichiometry. In addition, we performed amide hydrogen−deuterium exchange (HDXMS) to determine the binding site,[17] and we present a structural model consistent with all of the data.

EXPERIMENTAL PROCEDURES

Cloning, Expression, and Purification. ASB9(1−252) and ASB9(35−252) were cloned into the pHis8 vector with an N-terminal His8 tag. ASB9(1−252)D32A was generated by site-directed mutagenesis from the ASB9(1−252) construct. All ASB9 proteins were expressed in BL21(DE3) cells, grown to an OD_{600} of 0.7, and induced with 0.4 mM isopropyl β-D-1-thiogalactopyranoside (IPTG) overnight at 18 °C in M9ZN medium (M9 medium supplemented with 10 g/L NZ amine). The cell pellet was resuspended in phosphate buffer [50 mM sodium phosphate (pH 8.0) and 300 mM NaCl] containing 10 mM imidazole and 0.5 mM phenylmethanesulfonyl fluoride (PMSF), sonicated on ice, and centrifuged for 30 min at 12000 rpm. The supernatant was loaded over a 10 mL Ni-NTA (His-Pur, Pierce) column at 4 °C, washed with phosphate buffer containing 50 mM imidazole, and eluted with phosphate buffer containing 250 mM imidazole. Fractions containing ASB9 were pooled and dialyzed into 20 mM Tris (pH 8.5), 200 mM NaCl, 0.5 mM EDTA, and 1 mM DTT. Aliquots (2 mL) of the dialyzed protein were flash-frozen in liquid nitrogen, stored at −80 °C, and further purified on a Superdex-200 (S-200) gel filtration column before each experiment (GE Healthcare).

CKB was cloned in pET11a and expressed in BL21(DE3) cells, grown to an OD_{600} of 0.7, and induced with 0.4 mM IPTG overnight at 18 °C in M9ZN medium (M9 medium supplemented with 10 g/L NZ amine). The protein was purified over a blue Sepharose column as described previously.[18] The cells were resuspended in buffer A [10 mM MES (pH 6.0), 20 mM KCl, and 1 mM DTT] containing 0.5 mM PMSF, sonicated on ice, and centrifuged for 30 min at 12000 rpm. The supernatant was loaded onto a 50 mL blue Sepharose column at 4 °C and washed with 5 column volumes of buffer A, and CKB was eluted with 2 column volumes of buffer B [10 mM TES (pH 8.0), 20 mM KCl, and 1 mM DTT]. Fractions containing the enzyme were pooled and dialyzed into 50 mM HEPES, 0.1 mM EDTA, and 1 mM DTT (pH 7.0), and aliquots were stored at −80 °C. CKB fractions were also purified on a S-200 gel filtration column (GE Healthcare), and the eluted protein was concentrated in a 10 kDa molecular mass cutoff Amicon Ultra centrifugal filter (Millipore).

The complex (CKB+ASB9) was formed by mixing a 10 μM solution of ASB9 with a 15 μM (monomer concentration) solution of CKB to achieve a 1.14 ASB9:CKB monomer excess. The mixture was incubated for 2 h at 4 °C and purified by S200 size exclusion chromatography.

Activity Assay. Creatine kinase activity was determined by using a coupled enzyme assay as described previously.[19] The creatine kinase reaction is coupled to pyruvate kinase and lactate dehydrogenase reactions, and the conversion of NADH to NAD is observed at 340 nm to monitor the amount of creatine phosphate formed. Assays were performed at 30 °C in pH 9.0 triethanolamine buffer.[20] The assay mixture contained 0.2 mM NADH, 0.4 mM phosphoenolpyruvate, 5 mM ATP, 6 mM magnesium acetate, 13 mM potassium acetate, 28−56 units/mL pyruvate kinase, and 54−108 units/mL lactate dehydrogenase. The creatine kinase concentration was 3 nM (monomer), and the creatine concentration was varied from 10 to 100 mM. The assay mixture was incubated at 30 °C for 3 min, and the reaction was initiated by the addition of enzyme. The velocity of the reaction is calculated using an extinction coefficient of 6290 M^{-1} cm^{-1} for NADH. For assays testing the role of ASB9 binding in CKB activity, the complex (CKB +ASB9) was added to achieve a CKB concentration of 3 nM. V_{max} and K_M values were determined by fitting the data to the Michaelis−Menten kinetic model in Kaleidagraph (Synergy, Inc.).

Stoichiometry of the ASB9−CK Complex. Multiangle light scattering (MALS) analysis was performed to determine the stoichiometry of the ASB9−CK complex. In sequential runs, ASB9 alone, CK alone, and the ASB9−CK complex were analyzed. The proteins were buffer exchanged into 20 mM Tris (pH 8.0) and 100 mM NaCl, and 100 μL of a protein sample was analyzed via analytical size exclusion chromatography using a GE Healthcare Superdex 200 10/300 GL column with a flow rate of 0.4 mL/min. The column flowed directly into a miniDAWN TREOS MALS instrument (Wyatt Technology) and an Optilab UT-rEX instrument (Wyatt Technology). The Astra 6 instrument (Wyatt Technologies) was used to determine the weight-average molar mass of the eluting peaks using the intensity of the Rayleigh scattering as a function of scattering angle (LS) along with the buffer-subtracted refractive index (dRI).[21]

Measurement of Binding Thermodynamics. All isothermal titration calorimetry (ITC) experiments were performed on a VP-ITC calorimeter (MicroCal, Inc.). ASB9 constructs and CKB were purified by size exclusion chromatography on an S200 column in 50 mM bistrispropane (pH 8.5) and 200 mM sodium chloride, immediately prior to use. Protein concentrations were determined by measuring the absorbance at 280 nM and calculated using extinction coefficients as determined by amino acid analysis (for ASB9 constructs, ε = 24400 M^{-1} cm^{-1}; for CKB, ε = 33700 M^{-1} cm^{-1}). Experiments were performed at 30 °C; around 25 injections of 10 μL of 50 μM CKB dimer were made into 5 μM ASB9 in the cell. Isotherms were analyzed using Origin software (OriginLab) as described previously[22] and fit to a single-binding site model.

Measurement of Binding Kinetics. For surface plasmon resonance (SPR) experiments, CKB was cloned in pMCSG51 to add a biotinylation tag (Midwest Center for Structural Genomics). This plasmid has an N-terminal His tag to aid

DOI: 10.1021/bi501420n
Biochemistry 2015, 54, 1673−1680

purification, followed by an AVI tag that can be biotinylated on a specific lysine using *Escherichia coli* biotin ligase (BirA), which is co-expressed with the gene of interest. Biotinylated CKB was purified using a combination of Ni-NTA (using the phosphate buffers as the ASB9 constructs described above) and size exclusion chromatography over a S200 column. SPR experiments were performed on a Biacore 3000 instrument (GE Healthcare). Biotinylated CKB was immobilized on streptavidin (SA) chips in a high-salt buffer [50 mM HEPES (pH 8.0), 500 mM NaCl, 0.5 mM sodium azide, and 0.005% Tween 20]. Biotinylated CKB (300 RU) was immobilized on FC3 and data from FC1 (no CK immobilized) was automatically subtracted from FC3. Data collection rate set to high. The running buffer used for the binding experiments consisted of 50 mM HEPES (pH 8.0), 200 mM NaCl, 0.5 mM sodium azide, and 0.005% Tween 20. It is to be noted that ASB9 constructs have to be freshly purified by size exclusion chromatography and maintained at 4 °C for binding to be observed. Injections were made using the kinject mode at a rate of 20 μL/min, with a 240 s association time and a 300 s dissociation time for ASB9(35−252). The ASB9(35−252) concentration was varied from 0 to 20 nM. The data were analyzed using BiaEvaluation version 4.1 with a simple 1:1 Langmuir binding model.

Hydrogen−Deuterium Exchange Mass Spectrometry (HDXMS). HDXMS was performed on CKB, ASB9(1−252), ASB9(35−252), and CKB in complex with ASB9(1−252) and ASB9(35−252). Complexes were made by adding an excess of ASB9 to CKB and vice versa and incubating the complexes for 30 min at 4 °C. HDXMS experiments were conducted at Lilly, Inc., in San Diego, CA, using a Waters Synapt G2S system with H/DX technology as described previously,[23,24] with the exception that the quench buffer contained 100 mM phosphate, 2 M guanidine hydrochloride, and 320 mM TCEP (pH 2.4). Each sample (5 μL) was mixed with 55 μL of D_2O buffer (containing 0.1× PBS) for several deuteration times (10 s to 10 min) at 15 °C. The exchange was quenched for 2 min at 1 °C with an equal volume of quench buffer. A portion of the quenched sample (50 μL) was injected onto an online pepsin column (Applied Biosystems, Poroszyme Immobilized Pepsin cartridge). The resulting peptic peptides were then separated on a C18 column (Waters, Acquity UPLC BEH C18, 1.7 μm, 1.0 mm × 50 mm) fit with a Vanguard trap column using a 3 to 85% acetonitrile (containing 0.1% formic acid) gradient over 12 min at a flow rate of 40 μL/min. The separated peptides were directed into a Waters SYNAPT G2s quadrupole time-of-flight (qTOF) mass spectrometer. The mass spectrometer was set to collect data in the MS^E, ESI^+ mode; in a mass acquisition range of m/z 255.00−1950.00; with a scan time of 0.4 s. Continuous lock mass correction was accomplished with infusion of the LeuEnk peptide every 30 s (mass accuracy of 1 ppm for the calibration standard). The peptides were identified using PLGS version 2.5 (Waters, Inc.). The relative deuterium uptake for each peptide was calculated by comparing the centroids of the mass envelopes of the deuterated samples with the undeuterated controls using DynamX version 2.0 (Waters Corp.).

Molecular Modeling. The extended structure of the ASB9 intrinsically disordered N-terminal domain, ASB9(1−35), was generated on the basis of the amino acid sequence in Maestro. Eleven parallel simulations were performed using the AMBER ff99SB force field[25] in a TIP3P water box.[26] The simulated system contained a single copy of the 35-residue ASB9 N-terminus in an orthorhombic water box with dimensions of 67 Å × 63.63 Å × 64.36 Å, with periodic boundary conditions. The N-terminus and C-terminus of ASB9 were capped with acetyl and methyl groups, respectively. The total system contained 61016 atoms, including a low (0.15 M) concentration of sodium chloride in the water solvent. Simulations were performed with NVIDIA GK110 (GeForce GTX Titan) GPUs using the CUDA version of PMEMD in AMBER12.[27] The ASB9(1−35) system was relaxed using 86000 steps of energy minimization followed by one restrained 250 ps heating step up to 303 K. Three consecutive restrained 250 ps equilibration steps were performed. The restraint force was applied to the backbone atoms in these equilibration steps starting at 3.0 kcal $Å^{-2}$ mol^{-1} for the first step, then 2.0 kcal $Å^{-2}$ mol^{-1} for the second step, and 1.0 kcal $Å^{-2}$ mol^{-1} for the last step before the performance run. Long-range electrostatics were calculated using the particle mesh Ewald (PME) method,[28] with a 10 Å cutoff and a 1.2 Å grid spacing. Ten simulations were performed at 303 K for 25 ns each, for a total of 250 ns of sampling time. The trajectory structures were clustered using the GROMOS algorithm[29] in GROMACS version 4.5.5,[30] with a backbone root-mean-square deviation (rmsd) cutoff of 3.5 Å for ASB9(1−35). The top eight (90% of the total ensemble) cluster centroids were analyzed, and the most elongated and compact cluster centroids were appended onto the crystal structure of the ARD of ASB9.

The molecular model of ASB9(1−252) was built from the 2.2 Å crystal structure of splice variant 2 of the ARD of ASB9 from hASB9-2 [Protein Data Bank (PDB) entry 3D9H]. The top eight cluster centroids of the ASB9(1−35) simulation (representing 90% of the total ensemble) were analyzed, and the most elongated and compact cluster centroids were appended onto the crystal structure of the ARD of ASB9 in Maestro. The two models of ASB9(1−252), one with an elongated N-terminus and one with a compact N-terminus, were docked into two models of brain-type CK (CKB): the crystal structure of CKB (PDB entry 3DRB, which has one open monomer and one closed monomer)[31] and a model of the open−open CKB crystal structure generated in VMD by overlaying two crystal structures over one another. In VMD, the rmsd trajectory tool extension was used to align two CKB crystal structures.

The ZDOCK server was used to dock both models of ASB9 into both models of CKB (http://zdock.umassmed.edu/).[32] The top 10 structures of each of the four dockings were compared on the basis of their ZDOCK scores (1103−1778 points), the consistency of the binding interface determined from the rmsd of the docked orientation from the top 10 docked complexes, and the steric overlap of the SOCS box domain with CKBB when the ASB9−Elongin BC crystal structure (PDB entry 3ZNG)[8] is overlaid with the docked complexes.

RESULTS

The Affinity of the ASB9−CK Complex Requires Two Regions of ASB9. The affinity of the ASB9−CK complex was measured by both surface SPR and ITC. For these experiments, the binding affinity of the ARD of ASB9 [ASB9(35−252)] was compared to the affinity of a construct containing both the ARD and the 34 N-terminal residues. Both SPR and ITC revealed that the binding affinity between ASB9(1−252) and CK is extremely high. For ASB9(1−252), no dissociation was observed, even when 3 M guanidine hydrochloride was included in the dissociation buffer in the SPR experiments (Figure 1A). ITC experiments corroborated this observation.

DOI: 10.1021/bi501420n
Biochemistry 2015, 54, 1673−1680

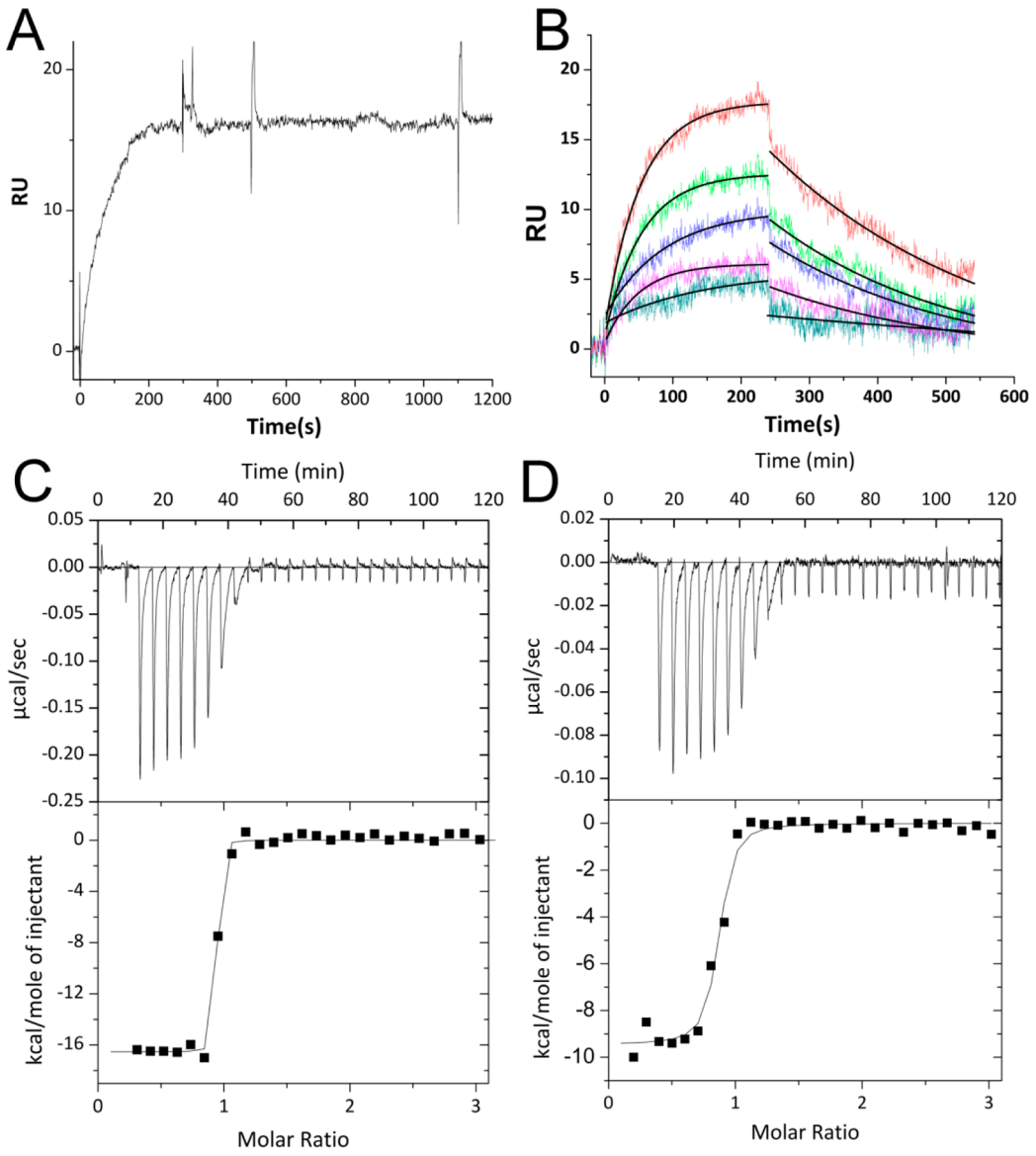

Figure 1. Measurement of binding kinetics and thermodynamics. (A) SPR experiment in which 30 nM ASB9(1−252) was passed over immobilized CKB at a rate of 20 μL/min. Regeneration was attempted by adding 3 M guanidine hydrochloride to the regeneration solution at 500 s, but no dissociation was observed. (B) SPR experiment in which 8, 9, 10, 12, and 14 nM ASB9(35−252) was passed over immobilized CKB at a rate of 20 μL/min. Regeneration was conducted with buffer containing 0.5 M guanidine hydrochloride and 10 mM ATP. The curves were fit globally using a 1:1 Langmuir binding model to yield the following binding constants: $k_d = 3.5 \times 10^{-3}$ s^{-1}, $k_a = 1.36 \times 10^6$ M^{-1} s^{-1}, and $K_D = 2.6 \times 10^{-9}$ M. (C) ITC thermogram and fit for 50 μM CKB (dimer concentration) (in the syringe) binding to 5 μM ASB9(1−252) (in the cell). Because the binding was so tight, only the ΔH could be determined from the data [−16.5 ± 0.2 kcal/mol (N = 0.9)]. (D) ITC thermogram and fit for 50 μM CKB (dimer concentration) (in the syringe) binding to 5 μM ASB9(35−252). For this truncated version of ASB9, ΔH = −9.9 ± 0.2 kcal/mol (N = 0.78).

Although the c value was too high to measure the K_d, the ΔH of the interaction was large, −16.5 kcal/mol, and could be determined with a high degree of precision (Figure 1C). Sensorgrams collected with immobilized CKB and ASB9(35−252) from 0 to 14 nM revealed a k_d of 3.5×10^{-3} s^{-1} and a k_a of 1.36×10^6 M^{-1} s^{-1}, yielding a K_D of 2.6×10^{-9} M (Figure 1B). Although the c value for this interaction was still high, the ΔH of the interaction was only −9.8 kcal/mol for the truncated version (Figure 1D). These results strongly suggested a bipartite interaction of ASB9 with CK.

Stoichiometry of the ASB9−CK Complex. CK is a dimeric protein, and therefore it was necessary to determine whether one molecule of ASB9 bound to a dimer of CK or whether each monomer of CK could bind an ASB9 molecule. Size exclusion chromatography and analytical ultracentrifugation experiments both suggested a stoichiometry of one ASB9 per CK dimer, but because of the elongated shape of ASB9, the results were inconclusive. MALS analysis of a mixture of CK with an excess of ASB9 showed conclusively that the stoichiometry was one ASB9 bound to one dimer of CK (Figure 2). The experiment was performed with an excess of ASB9, which eluted at the expected volume for monomeric ASB9.

Partial Inhibition of CK Activity by ASB9. The enzymatic activity of CK to form creatine phosphate was measured in a coupled assay.[19] In the absence of ASB9, the V_{max} was $(3.36 \pm 0.07) \times 10^{-7}$ M^{-1} s^{-1} (for comparison to literature values, this translated to a k_{cat} of 6.7×10^3 min^{-1}) and the K_M

DOI: 10.1021/bi501420n
Biochemistry 2015, 54, 1673−1680

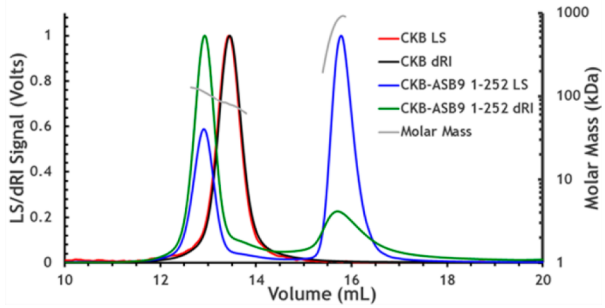

Figure 2. Multiangle light scattering (MALS) and refractive index curves for CKB and the CKB–ASB9 complex. The calculated molecular masses were 85.3 kDa for CKB, 29 kDa for ASB9(1–252), and 114 kDa for CKB and ASB9(1–252) (one CKB dimer and one ASB molecule). Both light scattering (LS) and refractive index with buffer subtracted (dRI) were measured and are plotted for each protein sample.

was 2.1 ± 0.2 mM. When the complex of ASB9(1–252) with CK was assayed, partial inhibition was observed so that the V_{max} of the complex was (2.1 ± 0.06) × 10^{-7} M^{-1} s^{-1} and the K_M was 3.4 ± 0.3 mM (Figure 3). This result was consistent with

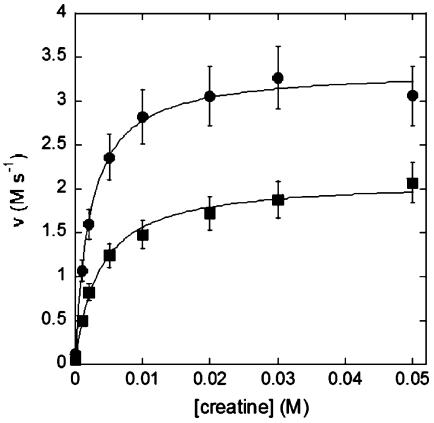

Figure 3. Enzyme activity of (■) CKB and (●) CKB with ASB9(1–252) at 3 nM enzyme and 30 °C. The K_M was 2.1 ± 0.2 mM, and the V_{max} was (3.36 ± 0.07) × 10^{-7} M^{-1} s^{-1} (for comparison to literature values, this translated to a k_{cat} of 6.7 × 10^3 min^{-1}). Binding of ASB9(1–252) to CKB partially inhibits the activity of CKB, increasing the K_M slightly to 3.4 ± 0.3 mM and decreasing the V_{max} to (2.1 ± 0.06) × 10^{-7} M^{-1} s^{-1}.

the MALS result that showed one ASB9 bound to a dimer of CK, likely leaving one active site available in the CK dimer. The complex of ASB9(35–252) with CK was also assayed, and this complex had full CK activity hinting that the N-terminus of ASB9 may occlude the active site of one monomer of CK in the ASB9(1–252)–CK complex.

HDXMS Mapping of the Interface between ASB9 and CK. To obtain information about where ASB9 and CK come in contact, amide hydrogen–deuterium exchange experiments (HDXMS) were performed in which the proteins were exposed to deuterated buffer for short periods of time to map the surface-exposed amides in the individual proteins and in the complex.[17] A Synapt G2S mass spectrometer was used for the study, yielding amide exchange measurements across nearly the entire sequence of both proteins (Figure 1 of the Supporting Information). These experiments revealed only one region of CKB, residues 182–203, was protected upon binding to ASB9(1–252) and ASB9(35–252). This region was covered by two peptides, 182–192 and 193–203, both of which showed a decreased level of exchange in the complex (Figure 4A–C).

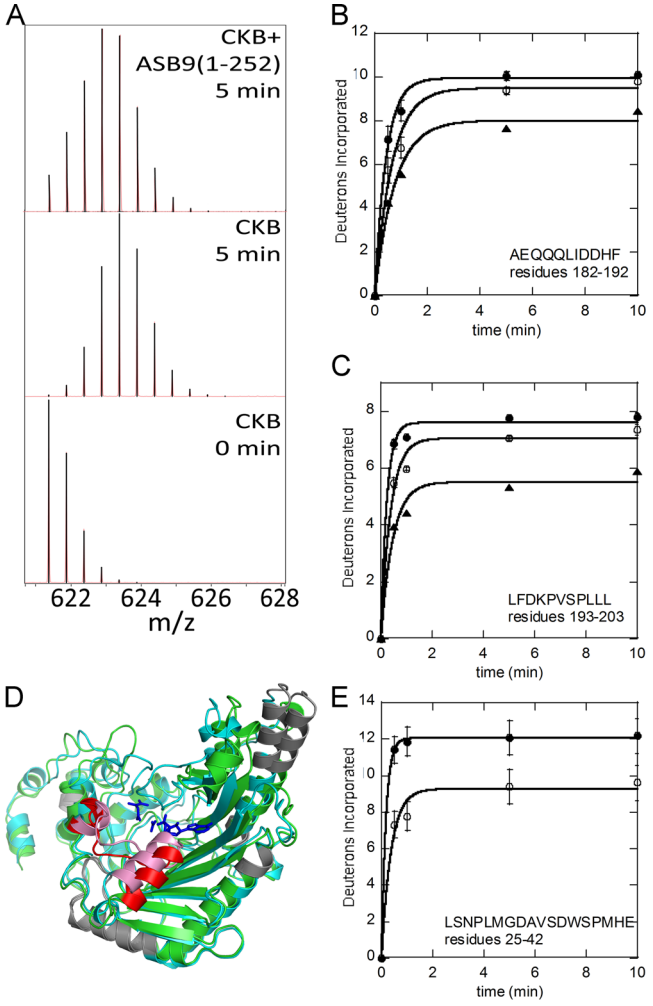

Figure 4. Amide hydrogen–deuterium exchange (HDXMS) results. (A) Peptide mass envelope for the CKB peptide LFDKPVSPLLL from CKB alone or in complex with ASB9(1–252) after exchange for 5 min showing a clear decrease in the level of deuterium uptake upon binding to ASB9. (B and C) D_2O uptake curves for CKB peptides AEQQQLIDDHF and LFDKPVSPLLL for (●) CKB, (○) CKB with ASB9(35–252), and (▲) CKB with ASB9(1–252). (D) Overlay of structures of human apo CKB (open, green) and CKB (closed, cyan) bound to Mg-ADP, NO_3 (shown as blue sticks), and creatine (shown as blue sticks). The region of CKB that shows a difference in deuterium incorporation upon binding to ASB9 is colored red in the open conformer and pink in the closed conformer. CKB regions that had no coverage are colored gray. (E) Deuterium uptake plot for the ASB9 peptide LSNPLMGDAVSDWSPMHE for (●) ASB9(1–252) and (○) ASB9(1–252) with CKB.

The protected residues 182–203 mapped to a helix–coil–helix region that is located right in front of the substrate-binding pocket of the CK active site (Figure 4D). The helix, residues 182–189, undergoes a conformational change and closes upon substrate binding as shown by the overlay of the two monomers from the dimeric CK crystal structure (PDB entry 3DRB).

The HDXMS results for ASB9 showed subtle changes throughout the protein; however, the main site of protection appeared to be N-terminal residues 25–42 (Figure 4E). A full

DOI: 10.1021/bi501420n
Biochemistry 2015, 54, 1673–1680

analysis of the HDXMS data on ASB9 will be presented in a separate study.

Molecular Modeling. Although a model of the ASB9−CK interaction has already been proposed,[13] this model was created from the crystal structure of ASB9 in which the first 35 residues were not observed, likely because of the N-terminus being disordered. As our binding studies implicated the N-terminus of ASB9 as a major contributor to binding affinity, we sought to model the disordered N-terminus and predict a model that included these residues. Multiple simulations of the N-terminal residues, ASB9(1−35), were performed, and the structures were clustered. Two clusters emerged from these simulations, one in which the N-terminus was extended and another in which it was folded back on itself. Representative models from these two cluster families were then attached to ASB9 to form a model of the full-length protein to create two different models of full-length ASB9. To explore whether it is the open state of CK or the closed state, two different models of the CK dimer were used. One corresponded to the CK crystal structure (PDB entry 3DRB) in which the A chain has an open active site and the B chain has the active site closed (and an ADP bound, which was removed for the docking). A second model in which both active sites were open was created starting again from the 3DRB structure but replacing the B chain (closed structure) with a replica of the A chain (open structure). The two different ASB9 models were docked against these two CK models, and the results of each trial were scored using a combination of the actual docking score from ZDOCK and the consistency of the docked orientation from the top 10 docked complexes. Only when the CK dimer in which both active sites were open was docked with ASB9 that had an extended N-terminus were consistent solutions with good ZDOCK scores obtained. The consistent solution from this docking trial mainly had the N-terminus and first ankyrin repeat of ASB9 docked between the two monomers of CK with the extended N-terminus lying in one of the CK active sites as was shown by a second scoring described in Experimental Procedures (Figure 5).

Role of Asp32 of ASB9. The molecular docking revealed a possible role for Asp32 of ASB9 in inhibition of CK activity. The docked structure showed Asp32 taking the place of one of the phosphates of ATP in the active site (Figure 5C). To test the importance of this interaction, we prepared the D32A mutant of ASB9 and compared its activity to that of the wild type. ITC experiments revealed the mutant protein interacted with CK with a ΔH of −3.7 kcal/mol, even lower than the binding enthalpy for the N-terminal truncation ASB9(35−252) (Figure 6). Activity assays showed that the D32A mutant partially inhibited the activity of CK. Whereas ASB9(1−252) inhibited the V_{max} of CK by 38 ± 4%, ASB9(D32A) inhibited the V_{max} by 22 ± 3% and ASB9(35−252) did not inhibit the activity at all.

A

	CKB (open/open)	CKB (open/closed)
Elongated N-term ASB9	**Score range 1230-1778** RMSD: 3.4 +/- 1.6 100% without steric overlap	**Score range 1113-1405** RMSD: 9.8 +/- 6.2 83% without steric overlap
Compact N-term ASB9	**Score range 1200-1516** RMSD: 12.9 +/- 1.7 44% without steric overlap	**Score range 1108-1325** RMSD: 11.3 +/- 2.1 57% without steric overlap

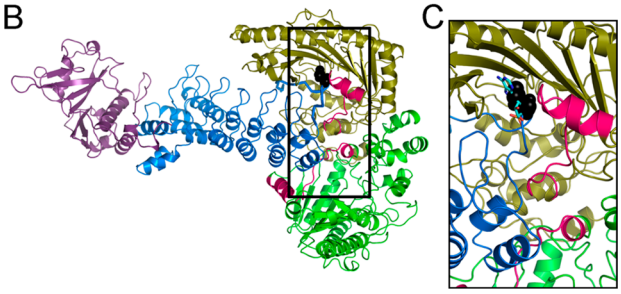

Figure 5. Best docked model of the ASB9−CK complex. (A) Table of results from docking of two different structural models of ASB9. One with an extended and the other with a collapsed N-terminus were docked with CKB structures that had either open or closed active sites. The solutions with the best ZDOCK score were obtained from the docking of the ASB9 with an extended N-terminus and an open CKB. The solutions were also overlapped with the ASB9−EloBC crystal structure (PDB entry 3ZKJ), and the percentage of structures that did not have steric clashes between the SOCS−EloBC and CKB structures is also reported in the table. RMSD is reported in Å. (B) Docked model of the ASB9(1−252)−CKB complex. The regions of CK (green and olive) that were shown to be protected upon ASB9 (blue) binding by HDXMS are colored bright pink. Aspartate 32 within the disordered N-terminus in ASB9 that binds in the ATP-binding pocket of CK is shown as black spheres. Elongin BC, which binds at the other end of the ASB9 ARD, is colored purple. (C) Close-up view of the active site of the CK monomer in which the N-terminus of ASB9 docks. The pose is the same as in panel B, but the ATP has been added back into the structure to show the superposition of Asp32 with the ATP.

DISCUSSION

In order to build up a functional model of how ASB9 interacts with CK, we performed a number of experiments and interpreted these in light of a docked molecular model. First, we found that one molecule of ASB9 interacts with a dimer of CK in an asymmetric manner. The N-terminus of ASB9 and the first ankyrin repeat nestle into the cleft between the two monomers of CK. The HDXMS data reveal a single region of CK that is protected from exchange in the complex, residues 182−203. This helix−strand−helix structure forms one lip of the CK active site and is known to undergo a conformational change, being open in the apoenzyme and closed in the substrate-bound form.[31]

Second, comparison of full-length ASB9(1−252) with an N-terminally truncated mutant, ASB9(35−252), revealed that both bound tightly, but the N-terminal residues made the affinity even higher. Interestingly, the N-terminal truncation, although it binds CK tightly, does not inhibit enzyme activity, and even full-length ASB9 only partially inhibits CK activity. Because of the stoichiometry of the complex (one ASB9 per dimer of CK), one active site remains open in the complex, and therefore, only partial inhibition is seen. Some studies have suggested that only one active site of CK functions at a time,[31] and our studies reveal that the ASB9−CK complex retains much of the CK activity. The partial inhibition seen is consistent with the docked model, which shows the disordered N-terminus of ASB9 lying in one active site with Asp32 interacting with the positively charged residues that normally interact with ATP. The D32A mutation shows partial inhibition consistent with weakening of this probably disordered interaction that would inhibit enzyme activity. Thus, it is

DOI: 10.1021/bi501420n
Biochemistry 2015, 54, 1673−1680

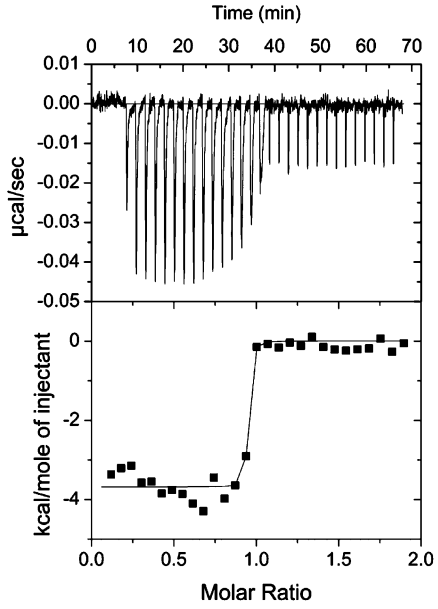

Figure 6. ITC thermogram and fit for 50 μM CKB (dimer concentration) (in the syringe) binding to 5 μM ASB9(1−252) D32A. For this mutant version of ASB9, $\Delta H = -3.7 \pm 0.08$ kcal/mol.

possible that CK could exist in cells as the ASB9 complex and still retain significant activity.

Third, we found that ASB9(1−252) interacts with CK so tightly that dissociation was not observed even in the presence of denaturant. This result is reminiscent of the interaction of IκBα with NFκB, for which dissociation is also not observed.[22,33] As with IκBα, this result suggests that proteasomal degradation is the only way to dissociate the complex.[34] The result also suggests that the ASB9−CK complex may be a stable subcomponent of the complete ECS-type CR E3 ligase. Studies of the other protein−protein interactions within the complex will reveal whether any of the other components weaken this interaction or whether the complex remains intact until proteasomal degradation occurs.

Our model of the ASB9−CK complex differs significantly from that predicted previously when only the crystallographically ordered portion of ASB9 was used in the docking.[13] We observed that the N-terminal residues contributed substantially to the binding based on ITC, SPR, HDXMS, and enzymatic assays. Therefore, we sought a way to predict some possible structures of the disordered N-terminus of ASB9 to generate a more realistic docked model.[13] Remarkably, the docked model we obtained, with the N-terminus included, was completely consistent with HDXMS data showing where the two proteins made surface contact. The C-terminus of ASB9, which must interact with Elongin BC and the rest of the ECS-type CR E3 ligase, protrudes from the center of the CK dimer placing the CK at the tip of the long ARD, almost like a lollypop on the end of a stick. Our model suggests that a simple hinging motion in the ECS-type CR E3 ligase would allow contact of the CK with the ubiquitin at the other end of the E3 ligase complex. Such a model is only one of several possible mechanisms for ubiquitin transfer requiring further study.

■ ASSOCIATED CONTENT

Ⓢ Supporting Information

Figure 1 showing all of the deuterium uptake curves for CK alone and in complex with ASB9(1−252) and ASB9(35−252). This material is available free of charge via the Internet at http://pubs.acs.org.

■ AUTHOR INFORMATION

Corresponding Author

*E-mail: ekomives@ucsd.edu. Phone: (858) 534-3058.

Funding

D.B. is supported by American Heart Association Postdoctoral Award 14POST18970079. J.S. is supported by National Institutes of Health (NIH) Molecular Biophysics Training Grant T32 GM008326-23. This work was funded in part through a NIH Director's New Innovator Award (DP2-OD007237) to R.E.A. and by NIH Grant P01 GM071862 to E.A.K. Support from the National Biomedical Computation Resource (NBCR, P41 GM103426) to R.E.A. is also gratefully acknowledged.

Notes

The authors declare no competing financial interest.

■ ABBREVIATIONS

CKB, brain-type creatine kinase; uMtCK, ubiquitous mitochondrial creatine kinase.

■ REFERENCES

(1) Hershko, A., and Ciechanover, A. (1998) The ubiquitin system. *Annu. Rev. Biochem. 67*, 425−479.

(2) Schulman, B. A., and Harper, J. W. (2009) Ubiquitin-like protein activation by E1 enzymes: The apex for downstream signalling pathways. *Nat. Rev. Mol. Cell Biol. 10*, 319−331.

(3) Zheng, N., Schulman, B. A., Song, L., Miller, J. J., Jeffrey, P. D., Wang, P., Chu, C., Koepp, D. M., Elledge, S. J., Pagano, M., Conaway, R. C., Conaway, J. W., Harper, J. W., and Pavletich, N. P. (2002) Structure of the Cul1-Rbx1-Skp1-F boxSkp2 SCF ubiquitin ligase complex. *Nature 416*, 703−709.

(4) Petroski, M. D., and Deshaies, R. J. (2005) Function and regulation of cullin-RING ubiquitin ligases. *Nat. Rev. Mol. Cell Biol. 6*, 9−20.

(5) Zimmerman, E. S., Schulman, B. A., and Zheng, N. (2010) Structural assembly of cullin-RING ubiquitin ligase complexes. *Curr. Opin. Struct. Biol. 20*, 714−721.

(6) Duda, D. M., Borg, L. A., Scott, D. C., Hunt, H. W., Hammel, M., and Schulman, B. A. (2008) Structural insights into NEDD8 activation of cullin-RING ligases: Conformational control of conjugation. *Cell 134*, 995−1006.

(7) Kohroki, J., Nishiyama, T., Nakamura, T., and Masuho, Y. (2005) ASB proteins interact with Cullin5 and Rbx2 to form E3 ubiquitin ligase complexes. *FEBS Lett. 579*, 6796−6802.

(8) Thomas, J. C., Matak-Vinkovic, D., Van Molle, I., and Ciulli, A. (2013) Multimeric Complexes among Ankyrin-Repeat and SOCS-box Protein 9 (ASB9), ElonginBC, and Cullin 5: Insights into the Structure and Assembly of ECS-type Cullin-RING E3 Ubiquitin Ligases. *Biochemistry 52*, 5236−5246.

(9) Muniz, J. R., Guo, K., Kershaw, N. J., Ayinampudi, V., von Delft, F., Babon, J. J., and Bullock, A. N. (2013) Molecular architecture of the ankyrin SOCS box family of Cul5-dependent E3 ubiquitin ligases. *J. Mol. Biol. 425*, 3166−3177.

(10) Debrincat, M. A., Zhang, J. G., Willson, T. A., Silke, J., Connolly, L. M., Simpson, R. J., Alexander, W. S., Nicola, N. A., Kile, B. T., and Hilton, D. J. (2007) Ankyrin repeat and suppressors of cytokine signaling box protein asb-9 targets creatine kinase B for degradation. *J. Biol. Chem. 282*, 4728−4737.

(11) Kwon, S., Kim, D., Rhee, J. W., Park, J.-A., Kim, D.-W., Kim, D.-S., Lee, Y., and Kwon, H.-J. (2010) ASB9 interacts with ubiquitous mitochondrial creatine kinase and inhibits mitochondrial function. *BMC Biol. 8*, 1−23.

DOI: 10.1021/bi501420n
Biochemistry 2015, 54, 1673−1680

(12) Fei, X., Zhang, Y., Gu, X., Qiu, R., Mao, Y., and Ji, C. (2009) Crystallization and preliminary X-ray analysis of the splice variant of human ankyrin repeat and suppressor of cytokine signaling box protein 9 (hASB9-2). *Protein Pept. Lett. 16* (3), 333−335.
(13) Fei, X., Gu, X., Fan, S., Yang, Z., Li, F., Zhang, C., Gong, W., Mao, Y., and Ji, C. (2012) Crystal Structure of Human ASB9-2 and Substrate-Recognitionof CKB. *Protein J. 31*, 275−284.
(14) Zhong, L., Ge, K., Zu, J. C., Zhao, L. H., Shen, W. K., Wang, J. F., Zhang, X. G., Gao, X., Hu, W., Yen, Y., and Kernstine, K. H. (2008) Autoantibodies as potential biomarkers for breast cancer. *Breast Cancer Res. 10*, R40-41−R40-48.
(15) Tokuoka, M., Miyoshi, N., Hitora, T., Mimori, K., Tanaka, F., Shibata, K., Ishii, H., Sekimoto, M., Doki, Y., and Mori, M. (2010) Clinical significance of ASB9 in human colorectal cancer. *Int. J. Oncol. 37*, 1105−1111.
(16) Uranbileg, B., Enooku, K., Soroida, Y., Ohkawa, R., Kudo, Y., Nakagawa, H., Tateishi, R., Yoshida, H., Shinzawa, S., Moriya, K., Ohtomo, N., Nishikawa, T., Inoue, Y., Tomiya, T., Kojima, S., Matsuura, T., Koike, K., Yatomi, Y., and Ikeda, H. (2014) High ubiquitous mitochondrial creatine kinase expression in hepatocellular carcinoma denotes a poor prognosis with highly malignant potential. *Int. J. Cancer 134*, 2189−2198.
(17) Mandell, J. G., Falick, A. M., and Komives, E. A. (1998) Identification of protein-protein interfaces by decreased amide proton solvent accessibility. *Proc. Natl. Acad. Sci. U.S.A. 95*, 14705−14710.
(18) Chen, L. H., White, C. B., Babbitt, P. C., McLeish, M. J., and Kenyon, G. L. (2000) A comparative study of human muscle and brain creatine kinases expressed in *Escherichia coli*. *J. Protein Chem. 19*, 59−66.
(19) Tanzer, M. L., and Gilvarg, C. (1959) Creatine and creatine kinase measurement. *J. Biol. Chem. 234*, 3201−3204.
(20) Wang, P. F., McLeish, M. J., Kneen, M. M., Lee, G., and Kenyon, G. L. (2001) An unusually low pK_a for Cys282 in the active site of human muscle creatine kinase. *Biochemistry 40*, 11698−11705.
(21) Trathnigg, B. (1995) Determination of MWD and Chemical Composition of Polymers by Chromatographic Techniques. *Prog. Polym. Sci. 20*, 615−650.
(22) Bergqvist, S., Croy, C. H., Kjaergaard, M., Huxford, T., Ghosh, G., and Komives, E. A. (2006) Thermodynamics reveal that helix four in the NLS of NF-κB p65 anchors IκBα, forming a very stable complex. *J. Mol. Biol. 360*, 421−434.
(23) Dembinski, H., Wismer, K., Balasubramaniam, D., Gonzalez, H. A., Alverdi, V., Iakoucheva, L. M., and Komives, E. A. (2014) Predicted disorder-to-order transition mutations in IκBα disrupt function. *Phys. Chem. Chem. Phys. 16*, 6480−6485.
(24) Fang, J., Nevin, P., Kairys, V., Venclovas, C., Engen, J. R., and Beuning, P. J. (2014) Conformational analysis of processivity clamps in solution demonstrates that tertiary structure does not correlate with protein dynamics. *Structure 22*, 572−581.
(25) Hornak, V., Abel, R., Okur, A., Strockbine, B., Roitberg, A., and Simmerling, C. (2006) Comparison of Multiple Amber Force Fields and Development of Improved Protein Backbone Parameters. *Proteins: Struct., Funct., Bioinf. 65*, 712−725.
(26) Jorgensen, W. L. (1982) Revised TIPS for simulations of liquid water and aqueous solutions. *J. Chem. Phys. 77*, 4156−4163.
(27) Salomon-Ferrer, R., Goetz, A. W., Poole, D., Le Grand, S., and Walker, R. C. (2013) Routine microsecond molecular dynamics simulations with AMBER: Part II: Particle Mesh Ewald. *J. Chem. Theory Comput. 9*, 3878−3888.
(28) Darden, T., York, D., and Pedersen, L. (1993) Particle mesh Ewald: An Nlog(N) method for Ewald sums in large systems. *J. Chem. Phys. 98*, 10089−10092.
(29) Baron, R., and McCammon, J. A. (2007) Dynamics, hydration, and motional averaging of a loop-gated artificial protein cavity: The W191G mutant of cytochrome c peroxidase in water as revealed by molecular dynamics simulations. *Biochemistry 46*, 10629−10642.
(30) Hess, B., Kutzner, C., Van Der Spoel, D., and Lindahl, E. (2008) GROMACS 4: Algorithms for highly efficient, load-balanced, and scalable molecular simulation. *J. Chem. Theory Comput. 4*, 435−447.
(31) Eder, M., Schlattner, U., Becker, A., Wallimann, T., Kabsch, W., and Fritz-Wolf, K. (1999) Crystal structure of brain-type creatine kinase at 1.41 Å resolution. *Protein Sci. 8*, 2258−2269.
(32) Pierce, B. G., Wiehe, K., Hwang, H., Kim, B. H., Vreven, T., and Weng, Z. (2014) ZDOCK Server: Interactive Docking Prediction of Protein-Protein Complexes and Symmetric Multimers. *Bioinformatics 30*, 1771−1773.
(33) Alverdi, V., Hetrick, B., Joseph, S., and Komives, E. (2014) Direct observation of a transient ternary complex during IκBα-mediated dissociation of NF-κB from DNA. *Proc. Natl. Acad. Sci. U.S.A. 111*, 225−230.
(34) Ferreiro, D. U., and Komives, E. A. (2010) Molecular Mechanisms of System Control of NF-κB Signaling by IκBα. *Biochemistry 49*, 1560−1567.

DOI: 10.1021/bi501420n
Biochemistry 2015, 54, 1673−1680